Article

Shape Memory Properties and Microstructure of FeNiCoAlTaB Shape Memory Alloys

Li-Wei Tseng [1,*], Po-Yu Lee [1], Nian-Hu Lu [2], Yi-Ting Hsu [3] and Chih-Hsuan Chen [2]

1 Department of Mechatronics Engineering, National Changhua University of Education, Changhua 50007, Taiwan
2 Department of Mechanical Engineering, National Taiwan University, Taipei 10617, Taiwan; chchen23@ntu.edu.tw (C.-H.C.)
3 Department of Materials Science and Engineering, National Taiwan University, Taipei 10617, Taiwan
* Correspondence: lwtseng@cc.ncue.edu.tw

Abstract: The three-point-bending shape memory properties, microstructure, and magnetic properties of $Fe_{40.95}Ni_{28}Co_{17}Al_{11.5}Ta_{2.5}B_{0.05}$ (at.%) alloys were investigated. The magnetic results showed a martensitic transformation in the samples that were aged at 700 °C for 6 and 12 h under the applied magnetic fields of 0.05 and 7 Tesla. The martensitic start temperature increased from −113 °C to −97 °C as aging times increased from 6 to 12 h. Increasing the magnetic fields from 0.05 to 7 Tesla, the transformation temperatures increased to a higher temperature. Both samples reach saturation magnetization (140 emu/g) under 7 Tesla. The 98.5% cold-rolled alloys that were annealed at 1250 °C for 0.5 h presented a strong <100> texture in the rolling direction with an average grain size of 360 μm. Increasing the annealing time to 1 h, the intensity of texture reduced from 31.61 to 23.19. The fraction of low angle grain boundaries (LABs) for the 98.5% CR samples after annealing at 1250 °C for 0.5 h and 1 h was about 24.6% and 16.1%, respectively. Three-point-bending results show that the sample aged at 700 °C for 6 h displayed 0.2% recoverable strain at a stress level of 800 MPa. Failure occurred before the 900 MPa cycle could be completed. The sample aged at 700 °C for 12 h shows no transformation before the applied stress level of 300 MPa. As the stress levels increase to 400 MPa, the sample shows the shape memory effect and displayed 0.8% recoverable strain at a stress level of 400 MPa. The samples are failures during the 500 MPa cycle. The observed recoverable strain values were lower than those that were theoretically predicted, which was possibly due to the larger volume fraction of high-angle grain boundary and the slightly lower than expected average grain size.

Keywords: iron-based shape memory alloys; FeNiCoAlTaB; shape memory property; recoverable strain

1. Introduction

Shape memory alloys (SMAs) possess both superelasticity and shape memory effects due to the martensitic transformation. Nickel–titanium (NiTi) SMAs are widely applied in the aerospace, biomedical, robotics, and actuator industries, among others. Although NiTi SMAs show good mechanical properties, their high material cost and difficulty in forming the metals limit their applications [1,2]. Recently, additive manufacturing (AM) of NiTi SMAs has been developed due to the ability to fabricate complicated structures, and laser welding and selective laser melting (SLM) can generally provide a better surface finish and dimensional accuracy [3]. Deng et al. [4] investigated dissimilar NiTi/Ti6Al4V alloys joints fabricated by conventional friction stir welding at different parameters. The joint samples showed that the tensile stress was 269 MPa and the elongation was 3.8% with welding parameters (travel speed of 23.5 mm/min and rotation speed of 475 rpm). Chen et al. [5] investigated the effects of post-weld heat treatment (PWHT) on the microstructure and mechanical properties of laser-welded NiTi/304SS joints with Ni filler. They found that when the PWHT temperature was at 850 °C, the weld metal possessed the highest microhardness value of 493 HV. The tensile strength was 643 MPa and elongation

was 12%. These techniques still need further investigation for industrial applications. On the contrary, iron-based SMAs have attracted research interest due to their low material cost and good workability.

Recently, two Fe-based SMAs were shown to have superelastic behavior: one involved FeNiCoAlXB (X: Ti, Nb, Ta) systems [6–10]; and the other involved FeMnAlNi systems [11–13]. It is particularly interesting that FeNiCoAlTaB SMAs that showed a superelastic strain of 13.5% and a tensile strength of 1.2 GPa. However, these excellent properties require three conditions. First, a strong rolling texture in the <100> direction is required to achieve a superelastic strain of 13.5%. Second, a grain size greater than 400 μm is required to reduce the grain boundary constraints. (3) $L1_2$ precipitates are required to strengthen the matrix and alter the transformation temperature [6].

Ma et al. [14,15] reported that heat treatment of a solution at 1300 °C for 24 h followed by aging at 600 °C for 90 h for single crystals of <100>-oriented $Fe_{41}Ni_{28}Co_{17}Al_{11.5}Ta_{2.5}$ (at.%) resulted in 3.75% and 2% recoverable strain in shape memory in tensile and compressive tests, respectively. The precipitate's volume fraction was 38%, and the size of precipitates was 5 nm. Czerny et al. [16,17] found that single crystals of FeNiCoAlTa aged at 700 °C for short periods resulted in a small size of precipitates at around 2–6 nm. When the aging time was increased to 5 h, a huge compressive strain of 15.7% was obtained at a test temperature of −200 °C.

Geng et al. [18] found that there are four types of transformation behaviors of FeNiCoAlTaB SMAs during the aging heat treatments based on measurements of the electrical resistivity (ER). The first type is that in which the martensitic transformation is not clearly observed when a sample is aged at 700 °C for less than 5 h. The second type is that in which the martensitic transformation is fully reversible for a sample that is aged at 700 °C for between 5 and 24 h. In the third type, when a sample is aged at 700 °C for between 24 and 168 h, the thermoelastic martensitic transformation is not fully reversible. The final type is that in which the martensitic transformation is not observed for a sample that is aged at 700 °C for more than 168 h.

Zhang et al. [19] investigated the effects of various cold deformation and aging conditions on the microstructure and superelastic behavior of FeNiCoAlTaB SMAs [17]. For the aging temperature of 600 °C, as the aging time reached 10 h, the β-NiAl (B2) phase started to accumulate at the grain boundaries. A sample that was cold-rolled followed by annealing at 1300 °C for 30 min and aged at 600 °C for 72 h showed a superelastic strain of 2.5% based on their study.

Zhao et al. [20] found that large quantities of intermetallics existed in FeNiCoAlTaB SMAs with a temperature of 1150 °C or 1200 °C when in solution. When the heat treatment temperature was 1250 °C or 1300 °C, intermetallics were not observed in the samples. In addition, microcracks appeared at the sample's surface for a sample solution treated at 1300 °C. An FeNiCoAlTaB sample with 98.5% of cold-rolling underwent solution heat treatment at 1250 °C for 1 h and was aged at 600 °C for 72 h; this sample showed a strong <100> texture. Regarding the superelastic properties, the tensile strength and recoverable strain were 885 MPa and 1.6%, respectively.

Fu et al. [21] investigated the effects of grain orientations on the superelastic properties of FeNiCoAlTaB SMAs aged at 700 °C for 6, 12, and 24 h. The alloys underwent a tensile test, and this resulted in 1.7% and 1% recoverable strain for samples that were annealed and treated at 1215 °C for 20 min, followed by aging at 700 °C for 6 h and 12 h. A sample that was aged for 24 h showed no superelastic behavior due to the formation of precipitates of a large size. The precipitate size was less than 3 nm for a sample that was aged for 1 h. When the aging time was increased to 6 h, the precipitate size was approximately 13 nm. The precipitate size increased to 20 nm for the sample that was aged for 24 h. A large size of precipitates deteriorates the ductility of a sample.

Choi et al. [22] demonstrated that FeNiCoAlTaB wires showed a superelastic strain of 7% and a tensile strength of 1200 MPa after undergoing heat treatment at 1300 °C for 1 h and subsequently being aged at 600 °C for 72 h. The size of the precipitates ranged from

3 to 10 nm, and the volume fraction of the precipitates was 30%. The superelastic strain and tensile strength of the aged samples were around 7% and 1.2 GPa. According to the results of a stress–temperature test, the Clausius–Clapeyron slope was 5.4 MPa/°C between −40 and 30 °C. The brittle β-NiAl phases were not observed in either the high- or the low-angle grain boundaries in the oligocrystalline shape memory wires.

Zhang et al. [23] observed that $Fe_{40.95}Ni_{28}Co_{17}Al_{11.5}Ta_{2.5}B_{0.05}$ (at.%) alloys aged at 600 °C for 2 h displayed high tensile strengths in a wide range of temperatures. The tensile strengths are 2.2 GPa, 1.4 GPa, and 500 MPa at −196 °C, room temperature, and 800 °C, respectively. The precipitate's size ranges from 3 to 7 nm and the volume fraction of precipitates is around 28.2%. FeNiCoAlTaB wires showed superelastic properties with 1.8% superelastic strain at −196 °C.

In the present study, $Fe_{41.26}Ni_{28.2}Co_{17}Al_{11}Ta_{2.5}B_{0.04}$ (at.%) polycrystalline alloys were studied for their microstructure, magnetic properties, and shape memory behavior during a three-point-bending test.

2. Materials and Methods

High purities of Fe, Ni, Co, Al, Ta, and B raw materials (≥99.9 wt%) were used for the shape memory alloy used in this study. The regular 20 Kg ingots of equiatomic $Fe_{40.95}Ni_{28}Co_{17}Al_{11.5}Ta_{2.5}B_{0.05}$ (at.%) alloys' ingots were prepared by vacuum induction melting (VIM) and then cast into test bars. The pouring and mold temperatures were 1480 °C and 1100 °C, respectively. A bar was cut into several blocks by using wire electrical discharge machining (EDM). The dimensions of the blocks were as follows: length = 100 mm, width = 25 mm; and thickness = 25 mm. The blocks were prepared for a cold-rolling test.

The thermomechanical processing of $Fe_{40.95}Ni_{28}Co_{17}Al_{11.5}Ta_{2.5}B_{0.05}$ (at.%) alloys is shown in Figure 1. The procedure is presented in the following.
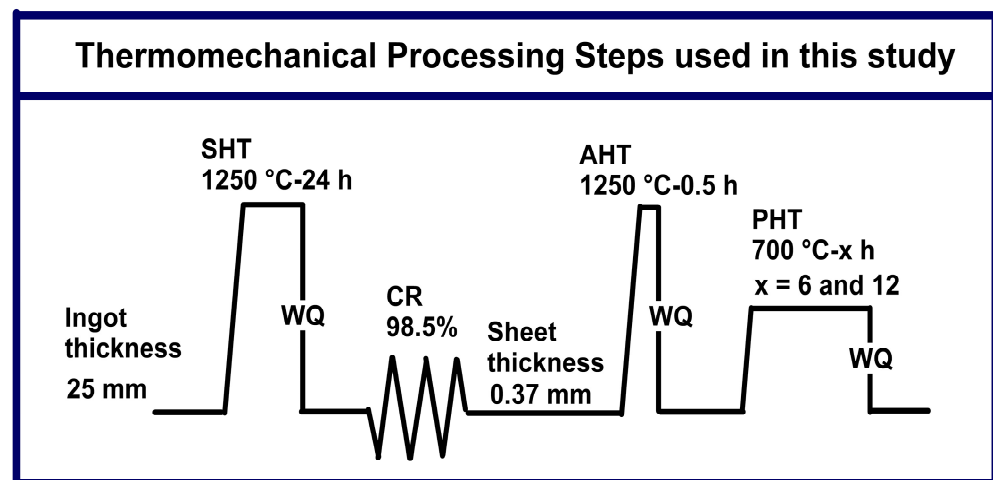
Figure 1. Illustration of the thermomechanical processes used to obtain $Fe_{40.95}Ni_{28}Co_{17}Al_{11.5}Ta_{2.5}B_{0.05}$ (at.%) alloy sheets. SHT, WQ, CR, AHT, and PHT indicate solution heat treatment, water quenching, cold-rolling, annealing heat treatment, and aging heat treatment, respectively.

In the first stage, the sample underwent solution heat treatment (SHT) at 1250 °C for 24 h (h) and was then water quenched (W.Q.). This stage was used to homogenize the block.

In the second stage, the block was cold-rolled (CR) to achieve a reduction of 98.5%, resulting in a thickness of 0.37 mm. Three-point-bending specimens were cut from the cold-rolled sheets.

In the third stage, the sample underwent annealing heat treatment (AHT) or a second solution heat treatment at 1250 °C for 0.5 h to obtain a recrystallized texture.

In the final stage, the sample was aged or underwent precipitation heat treatment (PHT) at 700 °C for 6 h and 12 h to obtain $L1_2$ precipitates (designated as 700 °C-6 h and 700 °C-12 h).

An Olympus digital optical microscope was used to observe the microstructures of the FeNiCoAlTaB samples. The composition of the etching solution was 7% nitric acid and 93% distilled water. Inductively coupled plasma mass spectrometry (ICP-MS) was used to analyze the composition of the FeNiCoAlTaB alloys. Vickers microhardness values were measured on the polycrystals at room temperature.

An X-ray diffractometer with Cu–Kα radiation was used to observe the crystal structures of the as-cast samples, the 98.5% CR samples, and the samples that underwent 98.5% CR and annealing at 1250 °C for 0.5 h. After 98.5% cold-rolling and solutionization, electron backscatter diffraction (EBSD) was used to investigate the texture evolution and low-angle grain boundary with a JeoL JSM-7800F instrument. The composition of the electropolishing solution for the sample surface was 90% C_2H_5OH + 10% $HClO_4$.

The magnetic properties of the FeNiCoAlTaB alloys that were aged at 700 °C for 6 and 12 h were determined by superconducting quantum interference device (SQUID) under magnetic fields of 0.05 and 7 Tesla. The cooling and heating rates were set to 5 K/min. The temperatures were between 120 °C and −260 °C. This test was used to determine the transformation temperatures of the FeNiCoAlTaB alloys.

The shape memory properties in three-point bending for 98.5% cold-rolled FeNiCoAlTaB samples after annealing at 1250 °C for 0.5 h and aging at 700 °C for 6 and 12 h were tested with an ElectroForce 3230 machine. The support span of the test machine was 20 mm. The test procedure was as follows: the first stress level was 100 MPa, and the temperature ranged from −150 °C to room temperature in one cycle; when a thermal cycle was completed, the applied stress level increased 100 MPa, and the next cooling/heating cycle was performed.; this process was repeated while increasing stress levels until the sample underwent failure.

3. Results

3.1. Microstructure and Composition Analysis Results

Figure 2a shows the 98.5% CR FeNiCoAlTaB sample. After 98.5% of the cold rolling deformation, the microstructrue shows the blurred grain boundaries. The reason is that thre large percentage of rolling reduction intensified the reifnemnt of grains, and the same observation is reported in FeNiCoAlNbB [24]. Figure 2b presents the 98.5% CR sample after annealing heat treatment at 1250 °C for 0.5 h. Grain boundaries appeared under these conditions. Figure 2c,d displays the annealed samples aged at 700 °C for 6 and 12 h. According to the results obtained for the microstructure, as the aging time increased to 12 h, β-NiAl phases were observed and these phses are first formed at the grain boundaries. The analysis of the composition of the 98.5% CR sample and the 98.5% CR sample annealing at 1250 °C for 0.5 h is shown in Table 1. In comparison with the nominal composition reported in [4], the sample that underwent annealing heat treatment had a higher Fe content and lower Ta and Al contents.

Table 1. Analysis of the composition of the FeNiCoAlTaB alloys.

Sample Condition	Fe	Ni	Co	Al	Ta	B
98.5% CR	45.57	25.9	16.32	9.74	2.43	0.04
98.5% CR + 1250 °C-0.5 h	45.5	27.16	16.83	8.38	2.08	0.05
nominal composition [4]	40.95	28	17	11.5	2.5	0.05
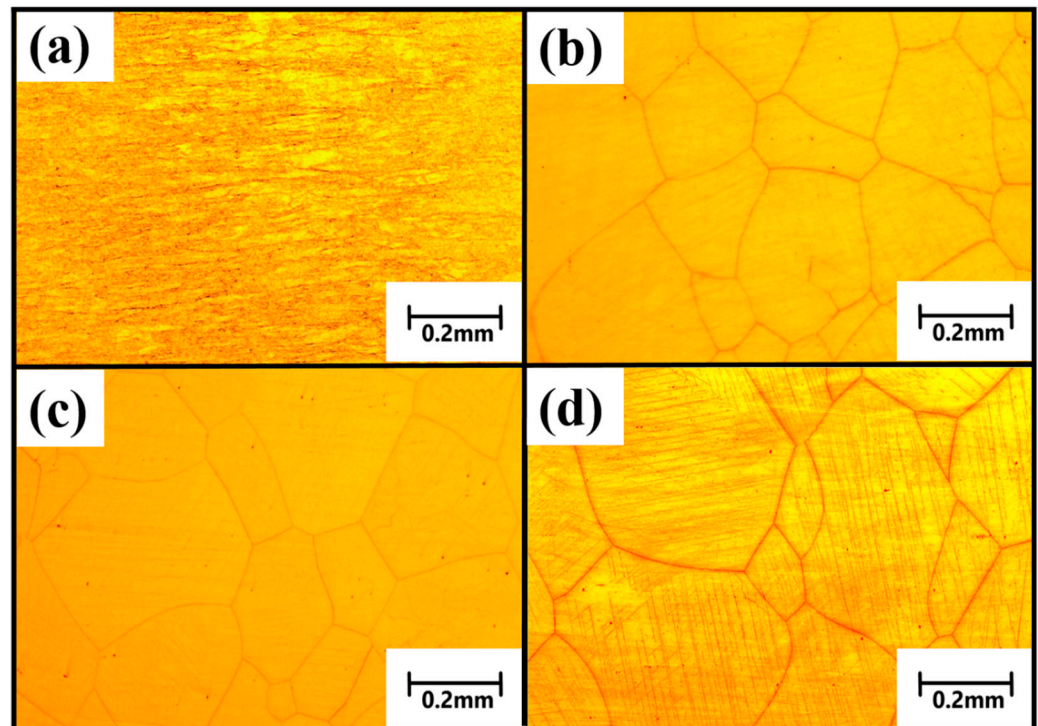
Figure 2. Microstructure of the FeNiCoAlTaB alloy under different thermomechanical processing conditions: (**a**) 98.5% CR, (**b**) 98.5% CR + 1250 °C-0.5 h, (**c**) 98.5% CR + 1250 °C-0.5 h + 700 °C-6 h, and (**d**) 98.5% CR + 1250 °C-0.5 h + 700 °C-12 h.

Table 2 displays the Vickers microhardness of the FeNiCoAlTaB alloys in various conditions. The microhardness value of the 98.5% CR specimen is 429 HV. The hardness of solution-treated sample is 223 HV. For the aging heat treatment condition, the microhardness values are 434 HV for 700 °C-6 h, 490 HV for 700 °C-12 h, and 424 HV for 700 °C-24 h. Increasing aging times to 12 h, the hardness values increase its values due to precipitation hardening. The hardness reaches peak value for 700 °C-12 h sample. The microhardness values decrease for the 700 °C-24 h due to overaged condition.

Table 2. Microhardness results of the FeNiCoAlTaB alloys in various conditions.

Thermo-Mechanical Processing	Vickers Hardness (HV)
98.5% CR	429 ± 9
98.5% CR + 1250 °C-0.5 h	223 ± 5
98.5% CR + 1250 °C-0.5 h + 700 °C-6 h	434 ± 6
98.5% CR + 1250 °C-0.5 h + 700 °C-12 h	490 ± 4
98.5% CR + 1250 °C-0.5 h + 700 °C-24 h	424 ± 8

3.2. X-ray Diffraction Results

The XRD patterns of the FeNiCoAlTaB samples at various conditions are shown in Figure 3. The samples' conditions are as-cast, 98.5% CR, and 98.5% CR + 1250 °C-0.5 h. It can be seen that the FCC, BCC, and Al_3Fe phases existed in the as-cast specimen. The cold-rolled samples that underwent the 1250 °C-0.5 h treatment showed a strong peak intensity of (111) plane. The FCC phase is the austenite phase. Using the (111) plane, the lattice parameter of the austenite phase is calculated to be 0.3619 nm and this value is not too different from the reported value of 0.3604 nm [6].
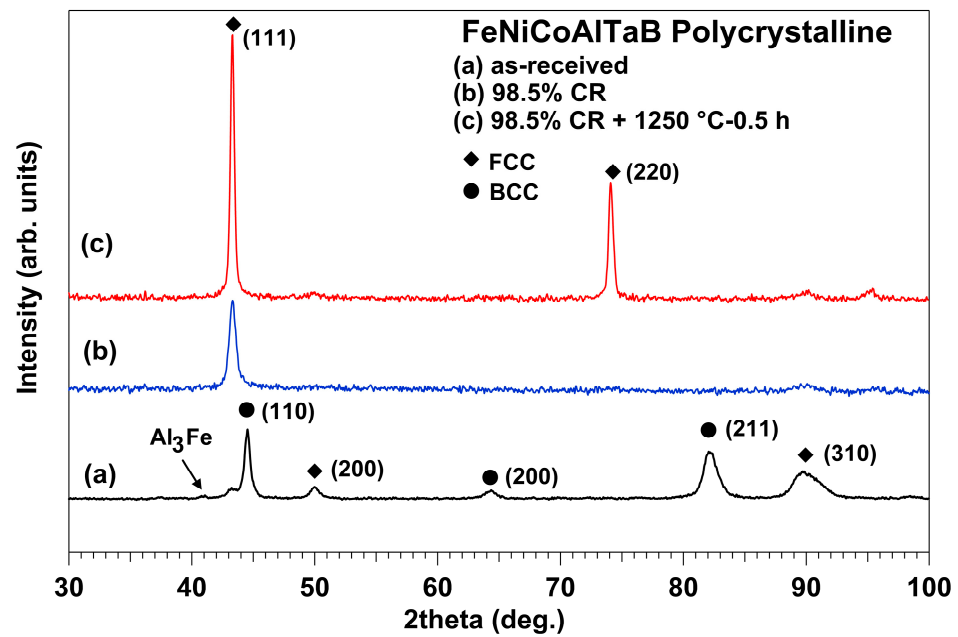
Figure 3. XRD patterns for the FeNiCoAlTaB samples at various conditions: as received, 98.5% CR, and 98.5% CR + 1250 °C-0.5 h.

3.3. Thermomagnetic Results

The martensitic transformation temperatures of the FeNiCoAlTaB aged specimens were obtained by using a thermomagnetic test. Figure 4a–d displays the temperature vs. magnetization responses under applied magnetic fields of 0.05 Tesla and 7 Tesla for the FeNiCoAlTaB samples for 700 °C-6 h and 700 °C-12 h aged samples. The transformation temperatures (A_f: austenite finish temperature; A_s: austenite start temperature; M_s: martensite start temperature; and M_f: martensite finish temperatures) were decided by using the tangent line method, as shown in Figure 4a,c. According to the results, A_f and A_s were −73 °C and −130 °C, respectively. M_f was −170 °C, and M_s was −113 °C. The temperature hysteresis (ΔT) was $|A_f–M_s|$ and was equal to 40 °C. For the 700 °C-12 h sample, the transformation temperatures were as follows: A_f = −50 °C; A_s = −106 °C; M_s = −97 °C; and M_f = −146 °C. ΔT = 47 °C.
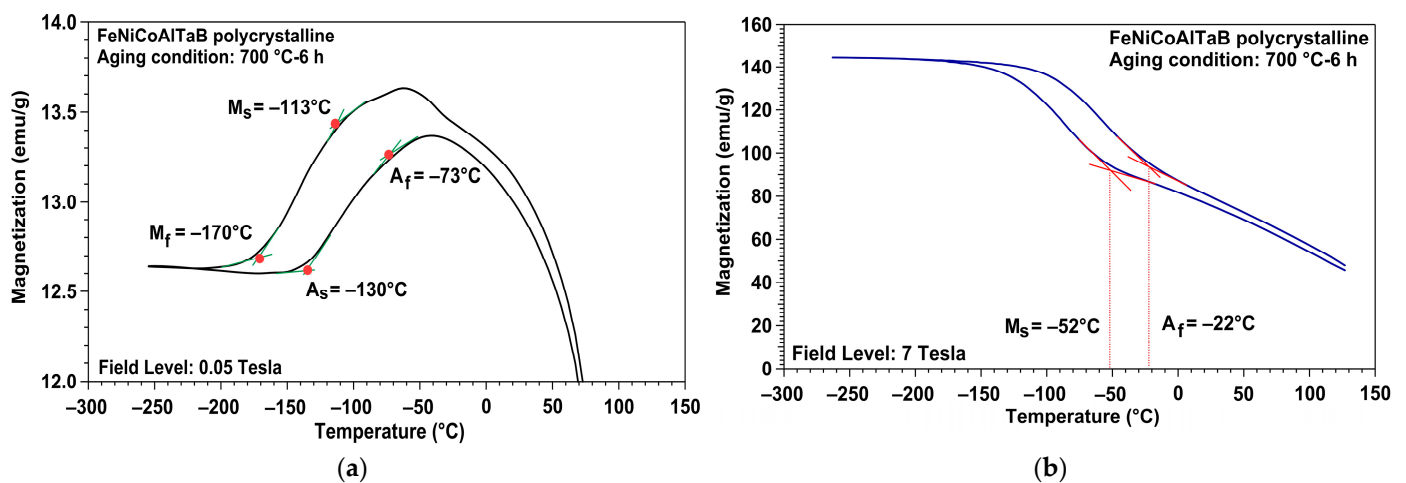
Figure 4. *Cont.*
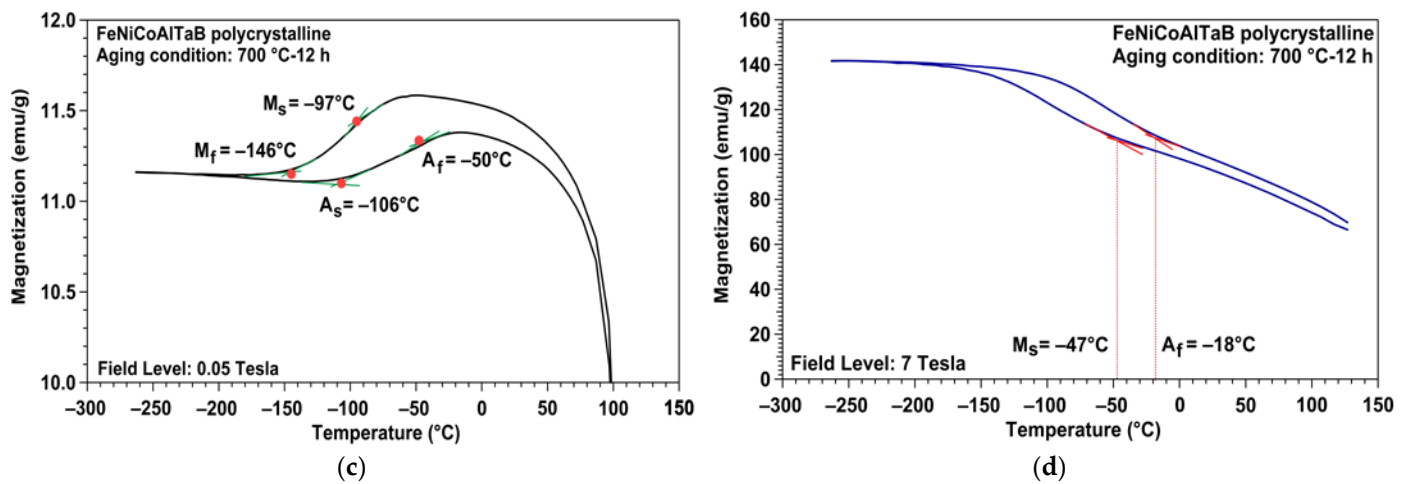
Figure 4. Magnetization response of the aged FeNiCoAlTaB samples. (**a**,**b**) 0.05 and 7 Tesla for 700 °C and 6 h; (**c**,**d**) 7 Tesla for 700 °C and 12 h.

Figure 4b,d shows the magnetic results under 7 Tesla for the FeNiCoAlTaB samples that were aged at 700 °C for 6 and 12 h. Both samples showed the same magnetization of 140 emu/g. M_s and A_f were −52 °C and −22 °C, respectively, for 700 °C-6 h. For the 700 °C-12 h sample, M_s was −47 °C and A_f was −18 °C. The results indicated that the transformation temperatures increased with the increase in the aging time. A similar trend was reported in FeNiCoAlTa and FeNiCoAlTiNb SMAs when the aging times increase from 24 h to 72 h at 600 °C [12,25]. Table 3 summarizes the transformation temperatures and temperature hysteresis for the FeNiCoAlTaB alloys. According to the results, the transformation temperature was increased when the magnetic fields were increased from 0.05 to 7 Tesla. The temperature hysteresis was reduced as the magnetic field levels were increased.

Table 3. M_s and A_f and temperature hysteresis of the FeNiCoAlTaB alloys.

Aging Condition	Magnetic Field	Transformation Temperature	Temperature Hysteresis
700 °C-6 h	0.05 T	A_f = −73 °C and M_s = −113 °C	40 °C
700 °C-6 h	7 T	A_f = −52 °C and M_s = −22 °C	30 °C
700 °C-12 h	0.05 T	A_f = −50 °C and M_s = −97 °C	40 °C
700 °C-12 h	7 T	A_f = −47 °C and M_s = −18 °C	29 °C

3.4. EBSD Results

The microstructure and grain orientation of the 98.5% CR sample's annealing heat treatment at 1250 °C for 0.5 and 1 h were examined by using EBSD tests. Figure 5a,b shows a quasi-colored orientation map and inverse pole figure of the 98.5% cold-rolled sample's annealing heat treatment at 1250 °C for 0.5 h and 1 h for the rolling direction (RD), transverse direction (TD), and normal direction (ND). The color shows the crystal orientation of the sample. According to the results of EBSD, the 98.5% CR samples that were annealed at 1250 °C for 0.5 and 1 h had average grain sizes of 360 μm and 370 μm, respectively. According to the results of the inverse pole figure, the rolling direction showed a strong <001> orientation. The intensity of the texture for the 98.5% CR samples after annealing heat treatment at 1250 °C for 0.5 h was 31.61. As the annealing time increased to 1 h, the intensity of the texture decreased to 23.19. This result indicated that the intensity of the texture decreased as the annealing time was increased.
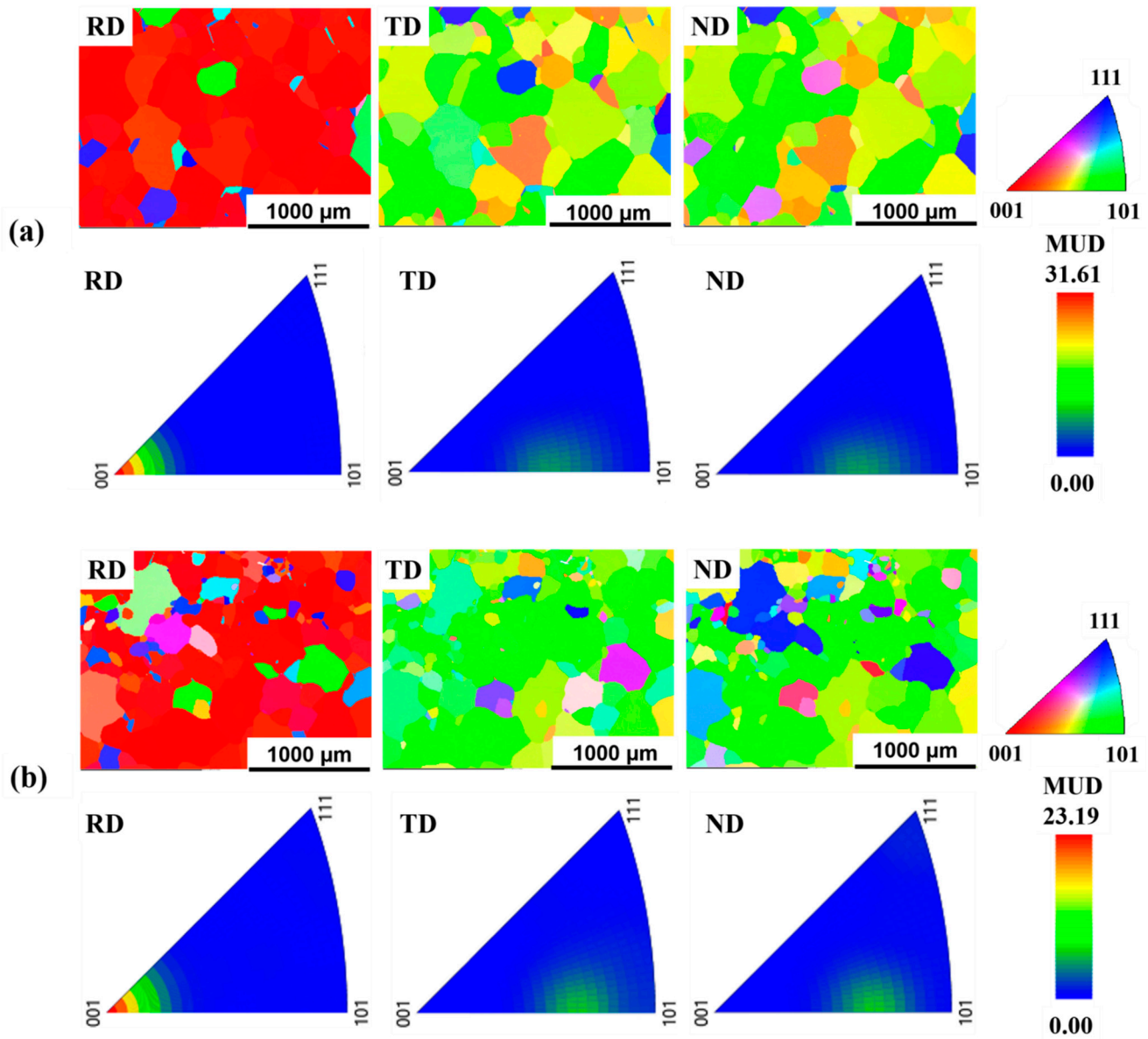
Figure 5. Quasi-colored orientation maps in the RD, TD, and ND of the 98.5% CR specimens after annealing treatment at 1250 °C for (**a**) 0.5 h and (**b**) 1 h.

3.5. Shape Memory Effect Test Results

Figure 6a shows that the shape memory properties, such as transformation temperatures and recoverable strain levels, were determined as a function of applied stress from a three-point-bending test. Figure 6b,c shows the three-point-bending results for 700 °C-6 h and 700 °C-12 h samples. The specimens aged at 700 °C for 6 h and 12 h showed no shape memory strain below a stress level of 600 MPa and 400 MPa, respectively. Figure 6d summarizes the recoverable strains at different applied stress levels for both 700 °C-6 h and 700 °C-12 h aged samples. Maximum recoverable strain is reached at 800 MPa for 700 °C-6 h aging specimens. The three-point-bending sample failed during the 900 MPa test. According to the result obtained with a stress level of 800 MPa, the maximum recoverable strain was around 0.2%. M_s was −54 °C and A_f was −23 °C. For 700 °C-12 h aged samples, the maximum recoverable strain (0.8%) was reached at 400 MPa. M_s and A_f were −90 °C and 0 °C, respectively. Failure occurred before the 500 MPa cycle could be completed. The linear relationships between applied stress and M_s and A_f temperatures were summarized in Figure 6e for the 700 °C-6 h aged sample. The stress M_s and A_f temperature slopes are

13 MPa/°C and 14 MPa/°C, respectively. The stress–temperature curves can be described by the Clausius–Clapeyron relationship:

$$\frac{d\sigma_c}{dT} = -\frac{\Delta S}{\varepsilon . V_m} \tag{1}$$

where $d\sigma/dT$ represents the critical stress–temperature slope; ΔS is the transformation entropy; V_m is the molar volume; and ε is the recoverable strain. The stress–temperature slope is inversely proportion to the recoverable strain. The higher stress–temperature slope implies that the sample shows a lower recoverable strain.
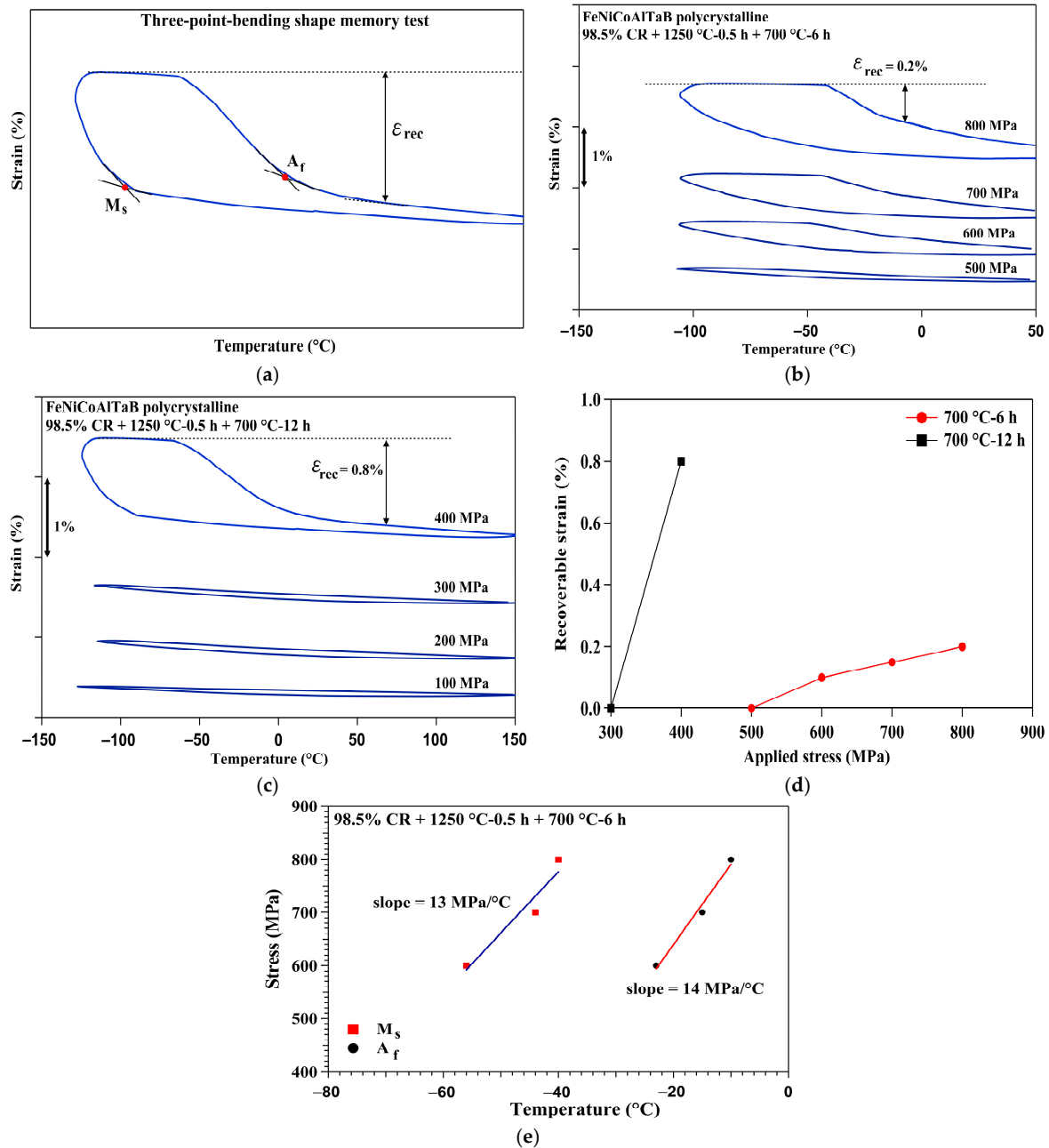
Figure 6. Shape memory properties of 700 °C-6 h and 700 °C-12 h aged samples in a three-point-bending test: (**a**) Demonstration of the method used to determine the recoverable strain and A_f and M_s temperatures; (**b**) 700 °C-6 h sample; (**c**) 700 °C-12 h sample; (**d**) recoverable strain vs. applied strain; and (**e**) stress vs. temperature slope for the A_f and M_s temperatures.

4. Discussion

According to the results of the shape-memory-bending test, the shape memory recoverable strain for the 700 °C-12 h specimen was smaller than the theoretical transformation strain for FeNiCoAlTaB SMAs [8]. One possible reason for this was the smaller fraction of low-angle grain boundaries (LABs). β phases cause the recoverable strain to be deteriorated and first form at high-angle grain boundaries (HABs). The development of LABs is important for suppressing the precipitation of β-NiAl at the grain boundaries. Figure 7a,b shows the grain boundary misorientation in the 98.5% CR alloys heat-treated at 1250 °C for 0.5 h and 1 h. These values were much smaller than those reported by Tanaka et al. [4]. Increasing the annealing time to 1 h decreased the percentage of LABs, and more β phases were generated along the grain boundaries. Tanaka et al. [4] found that the volume fraction of low-angle boundaries in FeNiCoAlTaB could reach almost 60%. In this study, as the fraction of LABs was 24.6% in the 98.5% CR sample solution-treated at 1250 °C for 0.5 h, β-NiAl phases still appeared in the textured sample due to the lower fraction of low-energy boundaries. As a result, the recoverable strain for the 700 °C-12 h specimen was smaller than the theoretically calculated value.
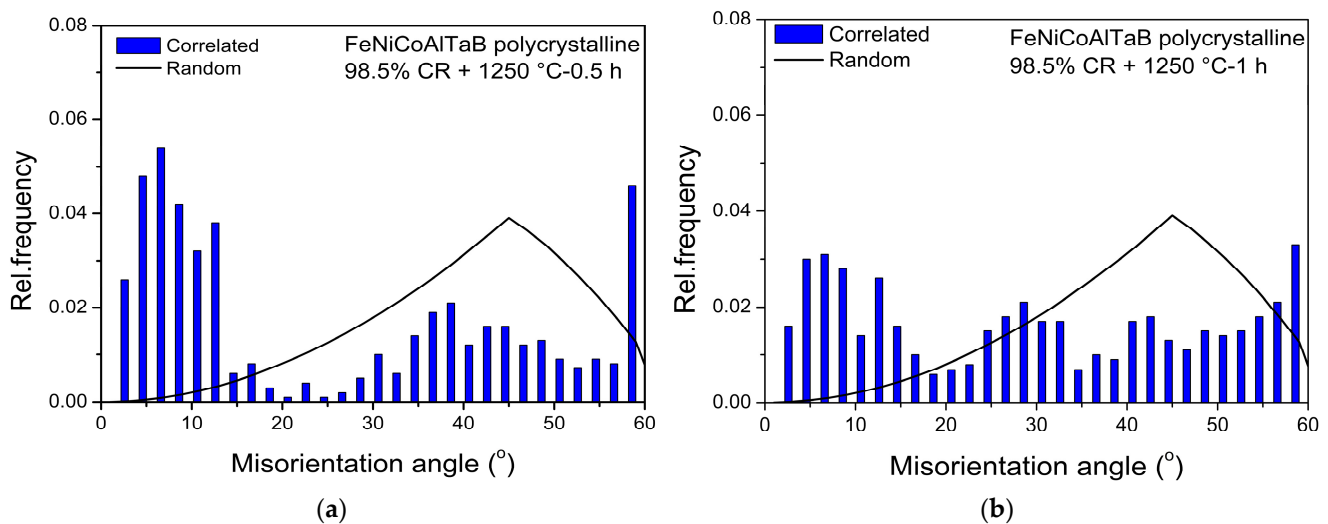
Figure 7. Grain boundary misorientation in the 98.5% CR specimens after annealing treatment at 1250 °C for (**a**) 0.5 h and (**b**) 1 h.

Furthermore, the grain size of this sample, which was found to be 360 μm, was smaller than the grain size of 400 μm reported by Tanaka et al. [4]. In iron-based SMAs, large grains are required to improve the mechanical properties due to the limited martensitic variants during the martensitic transformation [4]. A large grain size is effective for reducing the grain boundary constraint during shape memory tests. In this study, the grain size was lower than expected. As a result, the incompatibility between grains became more pronounced as the stress level was increased during the three-point-bending test, thus causing the specimens (aged for 6 h and 12 h) to break when the stress level was increased to 900 MPa and 500 MPa, respectively.

5. Conclusions

In the present work, the microstructure and shape memory behavior of cold-rolled FeNiCoAlTaB alloys were studied. We drew the following conclusions:

1. The 98.5% cold-rolled FeNiCoAlTaB alloy that underwent annealing treatment at 1250 °C for 0.5 h exhibited a strong intensity of texture, with 31.64 in the <100> orientation, and the average grain size was 360 μm. Increasing the annealing time to 1 h reduced the intensity of the recrystallized texture to 23.19. The fraction of LABs for

the samples after annealing at 1250 °C for 0.5 h was 24.6% and annealing at 1250 °C for 1 h was 16.1%;

2. Phase transformations were observed with the SQUID measurements under the magnetic fields of 0.05 and 7 Tesla for both 700 °C-6 h to 700 °C-12 h aging conditions. The martensitic start temperatures increased from -113 °C to -97 °C as the aging time was increased from 700 °C-6 h to 700 °C-12 h. Both aging samples reach the saturation magnetization of 140 emu/g when the magnetic field is 7 Tesla;

3. According to the three-point-bending result, the 700 °C-6 h and 700 °C-12 h samples exhibited a shape memory recoverable strain of 0.2% at a stress level of 800 MPa and 0.8% at a stress level of 400 MPa. The recoverable strains observed during three-point-bending were lower than the theoretically predicted values. The difference is believed to have been caused by the smaller fraction of LABs, as well as the slightly lower than expected grain size in the present study.

Data Availability Statement: Not applicable.

Conflicts of Interest: The authors declare no conflict of interest.

References

1. Otsuka, K.; Wayman, C.M. *Shape Memory Materials*; Cambridge University Press: Cambridge, UK, 1998; pp. 117–132.
2. Jani, J.M.; Leary, M.; Subic, A.; Gibson, M.A. A review of shape memory alloy research, applications and opportunities. *Mater. Des.* **2014**, *56*, 1078–1113. [CrossRef]
3. Wang, X.; Yu, J.; Liu, J.; Chen, L.; Yang, Q.; Wei, H.; Sun, J.; Wang, Z.; Zhang, Z.; Zhao, G.; et al. Effect of process parameters on the phase transformation behavior and tensile properties of NiTi shape memory alloys fabricated by selective laser melting. *Addit. Manuf.* **2020**, *36*, 101545. [CrossRef]
4. Chen, Y.; Sun, S.; Zhang, T.; Zhou, X.; Li, S. Effects of post-weld heat treatment on the microstructure and mechanical properties of laser-welded NiTi/304SS joint with Ni filler. *Mater. Sci. Eng. A* **2019**, *771*, 138545. [CrossRef]
5. Deng, H.; Chen, Y.; Jia, Y.; Pang, Y.; Zhang, T.; Wang, S.; Yin, L. Microstructure and mechanical properties of dissimilar NiTi/Ti6Al4V joints via back-heating assisted friction stir welding. *J. Manuf. Process.* **2021**, *64*, 379–391. [CrossRef]
6. Tanaka, Y.; Himuro, Y.; Kainuma, R.; Sutou, Y.; Omori, T.; Ishida, K. Ferrous polycrystalline shape-memory alloy showing huge superelasticity. *Science* **2010**, *27*, 1488–1490. [CrossRef] [PubMed]
7. Omori, T.; Abe, S.; Tanaka, Y.; Lee, D.; Ishida, K.; Kainuma, R. Thermoelastic martensitic transformation and superelasticity in Fe–Ni–Co–Al–Nb–B polycrystalline alloy. *Scr. Mater.* **2013**, *69*, 812–815. [CrossRef]
8. Lee, D.; Omori, T.; Kainuma, K. Ductility enhancement and superelasticity in Fe–Ni–Co–Al–Ti–B polycrystalline alloy. *J. Alloys Compd.* **2014**, *617*, 120–123. [CrossRef]
9. Tseng, L.W.; Ma, J.; Karaman, I.; Wang, S.J.; Chumlyakov, Y. Superelastic response of the FeNiCoAlTi single crystals under tension and compression. *Scr. Mater.* **2015**, *101*, 1–4. [CrossRef]
10. Chumlyakov, Y.I.; Kireeva, I.V.; Pobedennaya, P.; Krooβ, P.; Niendorf, T. Rubber-like behaviour and superelasticity of [001]-oriented FeNiCoAlNb single crystals containing γ- and β-phase particles. *J. Alloys Compd.* **2021**, *856*, 158158. [CrossRef]
11. Omori, T.; Ando, K.; Okano, M.; Xu, X.; Tanaka, Y.; Ohnuma, I.; Kainuma, R.; Ishida, K. Superelastic effect in polycrystalline ferrous alloys. *Science* **2011**, *333*, 68–71. [CrossRef]

12. Tseng, L.W.; Ma, J.; Wang, S.J.; Karaman, I.; Kaya, M.; Luo, Z.P.; Chumlyakov, Y.I. Superelastic response of a single crystalline FeMnAlNi shape memory alloy under tension and compression. *Acta Mater.* **2015**, *89*, 374–383. [CrossRef]

13. Tseng, L.W.; Ma, J.; Hornbuckle, B.; Karaman, I.; Thompson, G.B.; Luo, Z.; Chumlyakov, Y. The effect of precipitates on the superelastic response of [100] oriented FeMnAlNi single crystals under compression. *Acta Mater.* **2015**, *97*, 234–244. [CrossRef]

14. Ma, J.; Kockar, B.; Evirgen, A.; Karaman, I.; Luo, Z.; Chumlyakov, Y. Shape memory behavior and tension–compression asymmetry of a FeNiCoAlTa single-crystalline shape memory alloy. *Acta Mater.* **2012**, *60*, 2186–2195. [CrossRef]

15. Ma, J.; Hornbuckle, B.; Karaman, I.; Thompson, G.B.; Luo, Z.; Chumlyakov, Y. The effect of nanoprecipitates on the superelastic properties of FeNiCoAlTa shape memory alloy single crystals. *Acta Mater.* **2013**, *61*, 3445–3455. [CrossRef]

16. Czerny, M.; Cios, G.; Maziarz, W.; Chumlyakov, Y.; Chulist, R. Studies on the Two-Step Aging Process of Fe-Based Shape Memory Single Crystals. *Materials* **2020**, *13*, 1724. [CrossRef]

17. Czerny, M.; Maziarz, W.; Cios, G.; Wojcik, A.; Chumlyakov, Y.I.; Schell, N.; Fitta, M.; Chulist, R. The effect of heat treatment on the precipitation hardening in FeNiCoAlTa single crystals. *Mater. Sci. Eng. Mater. A* **2020**, *784*, 139327. [CrossRef]

18. Geng, Y.; Lee, D.; Xu, X.; Nagasako, M.; Jin, X.; Omori, T.; Kainuma, R. Coherency of ordered γ′ precipitates and thermoelastic martensitic transformation in FeNiCoAlTaB alloys. *J. Alloys Compd.* **2015**, *628*, 287–292. [CrossRef]

19. Zhang, C.; Zhu, C.; Shin, S.; Casalena, L.; Vecchio, K. Grain boundary precipitation of tantalum and NiAl in superelastic FeNiCoAlTaB alloy. *Mater. Sci. Eng. A* **2019**, *743*, 372–381. [CrossRef]

20. Zhao, H.; Fu, H.; Xie, J.; Zhang, Z. Effects of solution treatment on microstructure and superelasticity of FeNiCoAlTaB alloy. *Mater. Res. Express* **2018**, *5*, 016508. [CrossRef]

21. Fu, H.; Li, W.; Song, S.; Jiang, Y.; Xie, J. Effects of grain orientation and precipitates on the superelasticity in directionally solidified FeNiCoAlTaB shape memory alloy. *J. Alloys Compd.* **2016**, *684*, 556–563. [CrossRef]

22. Choi, W.S.; Pang, E.L.; Choi, P.P.; Schuh, C.A. FeNiCoAlTaB superelastic and shape-memory wires with oligocrystalline grain structure. *Scr. Mater.* **2020**, *188*, 1–5. [CrossRef]

23. Zhang, C.; Yu, Q.; Tang, Y.T.; Xu, M.; Wang, H.; Zhu, C.; Ell, J.; Zhao, S.; MacDonald, B.E.; Cao, P.; et al. Strong and ductile FeNiCoAl-based high-entropy alloys for cryogenic to elevated temperature multifunctional applications. *Acta Mater.* **2023**, *242*, 118449. [CrossRef]

24. Fu, H.; Zhao, H.; Shilei, S.; Zhang, Z.; Xie, J. Evolution of the cold-rolling and recrystallization textures in FeNiCoAlNbB shape memory alloy. *J. Alloys Compd.* **2016**, *628*, 287–292. [CrossRef]

25. Tseng, L.W.; Chen, C.H.; Chen, W.C.; Cheng, Y.; Lu, N.H. Shape memory properties and microstructure of new iron-based FeNiCoAlTiNb shape memory alloys. *Crystals* **2021**, *11*, 1253. [CrossRef]